applied optics

Apparatus and its principle for thermal aberration compensation

Xinfeng Yu,[1,2,*] Huaijiang Yang,[1] and Mingyang Ni[1]

[1]Changchun Institute of Optics, Fine Mechanics and Physics, Chinese Academy of Sciences, Dongnanhu Road, 3888#, 130033 Changchun, China
[2]University of Chinese Academy of Sciences, Beijing 100049, China
*Corresponding author: yu_xfeng@126.com

Received 19 May 2022; revised 11 September 2022; accepted 11 September 2022; posted 14 September 2022; published 3 October 2022

Thermal aberrations caused by absorption of laser beams degrade the image quality of exposure tools during the working process. Many compensators, such as lens movement or lens deformation, are used to compensate for low-order thermal aberrations of optical systems. In this paper, an apparatus with higher-order aberration correction capability is presented. The main principle of the apparatus is to actively heat and cool the lens near the pupil to generate a desired temperature profile to compensate for thermal aberrations. We first introduce the basic concept of the apparatus. Then we establish an analytical model to describe the lens temperature of the apparatus based on its working principle and demonstrate its compensation capability. Finally, an algorithm for dynamic thermal aberrations compensation is proposed to overcome the time lag effects of a thermally controlled lens.

https://doi.org/10.1364/AO.464483

1. INTRODUCTION

Due to the demand for lower-cost semi-conductor production, throughput and resolution of lithographic exposure tools have been continually improved over the past few decades. Various resolution enhancement techniques, such as off-axis illumination, have been applied in order to extend the resolution limit of the lithographic exposure tools. However, the use of extreme off-axis illumination combined with high scanner throughput leads to an obvious problem referred to as thermal aberrations [1–3]. Critical Dimension drift and overlay error are directly related to thermal aberrations. Thus, it is critical to control thermal aberrations during exposure.

Modern exposure tools from different manufacturers have been equipped with various manipulators to compensate for thermal aberrations. Nikon utilizes the "I-MAC" system to control low-order aberrations, such as magnification, distortion, coma, defocus, field curvature, and spherical aberrations by driving the lens element up and down in nanometer-level position accuracy. For other lower-order aberrations, such as constant astigmatism, Nikon has developed an infrared aberration control (IAC) system, which employs an infrared laser delivering thermal loads to the projection lens through optical hollow fibers, to heat the lens pupil selectively [1]. However, the IAC system could not provide a time-to-time response during compensation due to the heat capacity of the lens. To overcome this problem, deformable mirror "quick reflex" is used to compensate for constant astigmatism in a high numerical aperture (NA) system in S620D [4,5]. For higher-order aberration compensation, the "quick reflex 2" system, which is an extension of "quick reflex," has been developed in S631D. Its compensation capability is up to the 28th Zernike polynomial [6,7].

ASML has also developed many manipulators to compensate for thermal aberrations. In addition to lens motion as with Nikon's "I-MAC" system, an adaptive lens element was used in XT:1900i to compensate for constant astigmatism by deforming a specific lens through certain actuators [8]. To compensate for higher-order aberrations, such as Z6, Z10, Z17, etc., caused by exposure of rotated structures, an advanced lens controller is integrated in XT1950i [9]. The latest NA 1.35 immersion system applies a high-resolution wavefront manipulator called FlexWave with the correction capability of the Zernike series up to 64 terms [10]. The principle of the FlexWave manipulator is to actively steer a temperature profile on a transmissive optical element to modulate the wavefront of the optical systems.

There are many thermal controlling techniques applied in optical systems, such as the electrical heater [11–13] and infrared laser [1,14,15]. Methods for accurate establishment and validation of a thermal lensing model are also provided by many researchers [16–20]. However, when related to lithography, the techniques and models in the above-mentioned references could not be applied directly. A European patent [21] shows many embodiments of the wavefront manipulator FlexWave mentioned in Ref. [10]. In Ref. [21], the embodiments of the heating devices and optical arrangements of lenses are disclosed. However, the patent reveals no detailed principle

of the manipulator, especially how to establish a thermal model of such manipulator and compensate for dynamic thermal aberrations considering the heat capacity of the lens when thermal controlling techniques are used.

The goal of this paper is to provide a conceptual mechanical structure of the wavefront manipulator presented in Ref. [21] and try to establish a thermal model to describe the principle of the manipulator, especially how to compensate for dynamic thermal aberrations by modulating the heating power of each heating device.

This paper is organized as follows. In Section 2, we present the conceptual mechanical structure of the apparatus based on its working principle. In Section 3, we establish an analytical mathematical model of the apparatus for generating specific temperature profiles by modulating the heating powers of electrical heaters. In Section 4, a dynamic thermal aberration compensation algorithm of the apparatus is discussed, and compensation results are provided. Finally, the conclusions are discussed in Section 5.

2. CONCEPT OF THE APPARATUS

Thermal aberrations of the projection lens are mainly caused by a temperature-dependent index of refraction. However, we can thermally control the lens in an active way to compensate for the thermal aberrations.

The concept of the apparatus replicates the structure given in Figs. 4 and 9 of Ref. [21] with the dimension set by us, as shown in Fig. 1, and with the lens support structure and cooling channels added. As mentioned in Ref. [21], the apparatus is arranged near the pupil. The three lenses are arranged paralleled to the two confined channels. Both sides of the middle lens are covered by individually addressable heating devices. The heating devices might be made of tiny conductive wires that are small enough to keep the effects of obscuration and scattering negligible, and the heat dissipation of each heating zone can be adjusted. The number of heating devices is 256, and the size of each addressable heating zone is $6.5 \times 6.5\ \text{mm}^2$. The thickness of the middle lens covered by the heating devices is 4 mm, and its clear semi-aperture is 45 mm, which is smaller than the size covered by the heating devices. By guiding cooling fluid through the channel, such as N_2, the lens is cooled in parallel so that the lens can present a specific temperature profile.

It is preferred that the temperature of the cooling fluid be kept at the operating temperature of the exposure tools. Thus, the environment disturbance to the surrounding lens and the whole optical system can be minimized. However, in this way, the temperature of the lens element must be higher than the operating temperature of the exposure tools to make the lens have sufficient cooling power. There are two disadvantages in this way. First, a higher temperature of the lens element will transfer heat to the lens frame and further affects the temperature of adjacent lens frames. Secondly, surface deformation due to thermal expansion and the temperature rise itself will degrade the performance of the optical system.

To overcome the disadvantages mentioned above, a series of specific measures is implemented. To reduce heat transfer, an air gap (1 mm) was designed between the lens and the frame. At the same time, a cooling channel around the lens frame edge, as shown in Fig. 1(a), is provided to prevent heat from transferring to the outside of the lens frame. For the suppression of surface deformation, flexible supports are designed as shown in Fig. 1(b) to reduce the thermal stress between the frame and the lens. Since the middle lens in the apparatus should be heated to a higher uniform temperature than the operating temperature of the exposure tools, the image performance of the optical system will inevitably deteriorate. The image degradation might be corrected by other compensators in the projection lens or compensated for in advance at the design stage of the projection lens.

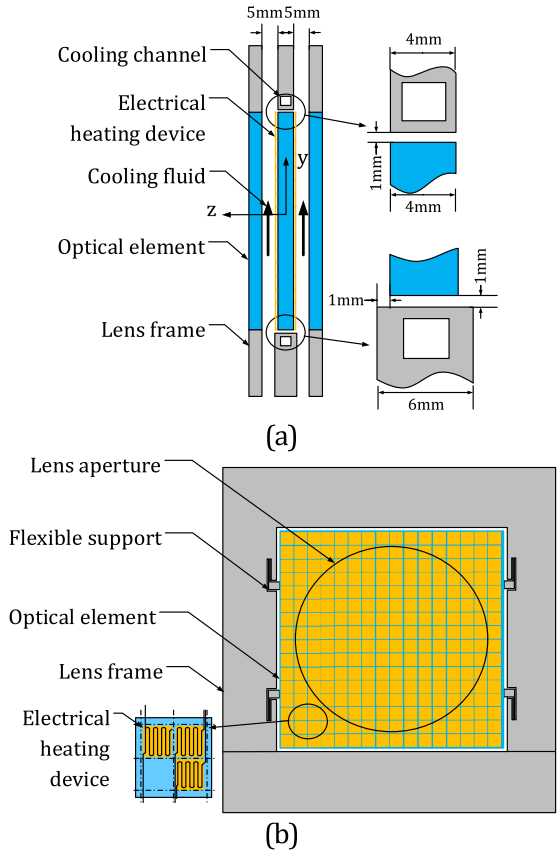

Fig. 1. Concept of the apparatus. (a) Section view of the apparatus and (b) front view of the apparatus.

Another noteworthy design, as shown in Fig. 1(a), is a lens frame in the incoming flow direction that is thicker than the lens. The step can effectively prevent the cold fluid from directly impinging on the hot lens, which avoids a large convective heat transfer coefficient near the edge of the lens.

3. PRINCIPLES OF THE APPARATUS

A. Heat Flux on the Surface of Lens

The cooling fluid flow in the channel is depicted in Fig. 2. The lens frame and the up lens are set to the working temperature of the optical system, such as 22°C, in accordance with the concept of the apparatus shown in Fig. 1. In order to get enough cooling power, the middle lens temperature is set to 26°C. A step of 1 mm is designed between the lens frame and the middle lens to prevent a large heat transfer coefficient at the edge of the lens.

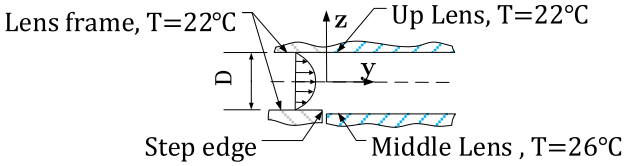

Fig. 2. Cooling fluid passing in the laminar flow in the channel.

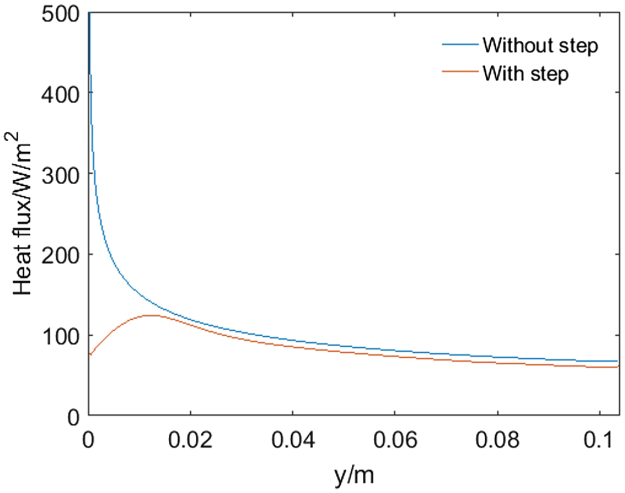

Fig. 3. Heat flux on each side of the middle lens.

Suppose that the cooling fluid in the channel is a two-dimensional flow and the mean velocity at the inlet is $v_0 = 3.0$ m/s; the Reynolds number of the channel of the incoming flow is

$$\mathrm{Re} = \frac{v_0 d_e}{\nu} \cong \frac{2 v_0 D}{\nu} = 1690 < 2300, \tag{1}$$

where d_e is the hydraulic diameter of the channel, and $D = 0.004$ m is the height between the lens frame at the inlet of the channel. $\nu = 1.42e-5$ m^2/s is the kinematic viscosity of N_2. We keep the flow laminar in the channel, which minimizes flow-induced vibration to the greatest extent.

According to the law of the laminar flow between parallel plates, the velocity at the inlet of the channel is given by

$$v(z) = \frac{2}{3} v_0 \left(1 - \frac{4z^2}{D^2}\right). \tag{2}$$

Using the boundary condition provided Fig. 2, a numerical simulation was implemented to obtain the heat flux on the surface of the lens. The heat flux on the middle lens surface is shown in Fig. 3 in the red line. The maximum heat flux on the lens surface is about 124 W/m^2, which is about twice the minimum. The flow with a step can greatly reduce the surface heat flux at the front of the lens compared to that without a step, as shown in Fig. 3 in the blue line.

B. Mathematical Model of Lens Temperature

Considering the cooling channel inside the lens frame around the lens, it is reasonable to approximate the lens frame temperature to 22°C. Therefore, the heat flux between the lens edge and the lens frame can be calculated by

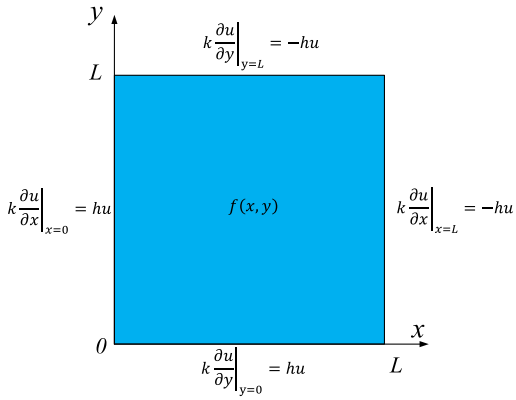

Fig. 4. Two-dimensional heat transfer model of the lens.

$$q = k\frac{\partial T}{\partial n} = -h(T - T_\infty),$$

where k is the heat conductivity of lens material, T is the temperature of the lens, T_∞ is the lens frame temperature, h is the heat transfer coefficient between the lens edge and the lens frame and calculated by $h = \lambda/\delta$, $\lambda = 0.0259$ W/(m · K) is the heat conductivity of N_2, and $\delta = 1$ mm is the air gap between the lens edge and the lens frame.

The z dimension of the lens is much smaller than the horizontal dimension, so the heat transfer model of the lens can be described in two dimensions, as shown in Fig. 4. The mathematical model of the lens temperature can be given as

$$\begin{aligned} &\frac{\partial u}{\partial t} = a\left(\frac{\partial^2 u}{\partial x^2} + \frac{\partial^2 u}{\partial y^2}\right) + \frac{a}{kd} f(x,y) \\ &k\frac{\partial u}{\partial x}\Big|_{x=0} = k\frac{\partial u}{\partial y}\Big|_{y=0} = hu,\ k\frac{\partial u}{\partial x}\Big|_{x=L} = k\frac{\partial u}{\partial y}\Big|_{y=L} = -hu \\ &u|_{t=0} = \phi(x,y), \end{aligned} \tag{3}$$

where $u = T - T_\infty$ is the excess temperature of the lens element over the reference temperature T_∞, $a = k/(\rho c_p)$ is the heat diffusivity of lens material, ρ is the density of lens material, c_p is the heat capacity of the lens, d is the thickness of the lens element, $f(x,y)$ is the heat flux on both lens surfaces, and $\phi(x,y)$ is the lens temperature at $t = 0$. It should be noted that the heat flux induced by the heating devices and cooling fluid on lens surfaces is represented in the form of bulk heat load in the mathematical model.

The analytical solution to Eq. (3) is

$$u(t,x,y) = \sum_{m=1}^{\infty}\sum_{n=1}^{\infty} T_{mn}(t) X_m(x) Y_n(y), \tag{4}$$

where

$$T_{mn}(t) = \phi_{mn} e^{-a(\alpha_m{}^2 + \beta_n{}^2)t} + \frac{\omega_{mn}}{a(\alpha_m{}^2 + \beta_n{}^2)}\left(1 - e^{-a(\alpha_m{}^2 + \beta_n{}^2)t}\right), \tag{5a}$$

$$\omega_{mn} = \frac{a\int_0^L\int_0^L X_m(x) Y_n(y) f(x,y)\,\mathrm{d}x\,\mathrm{d}y}{kd\|X_m(x)\|^2\|Y_n(y)\|^2}, \tag{5b}$$

Table 1. Material Properties of the Lens Used in the Apparatus[a]

Property	Unit	Value
Density ρ	kg/m^3	2201
Heat conductivity k	W/(m · K)	1.30
Heat capacity c_p	J/(kg · K)	741
Thermal coefficient dn_{ref}/dT at 193.40 nm	ppm/K	20.5

[a]Corning 7980.

$$\phi_{mn} = \frac{\int_0^L \int_0^L X_m(x) Y_n(y) \phi(x, y) \mathrm{d}x \mathrm{d}y}{\|X_m(x)\|^2 \|Y_n(y)\|^2}, \tag{5c}$$

$$X_m(x) = \sin(\alpha_m x) + \frac{k\alpha_m}{h} \cos(\alpha_m x), \tag{6}$$

$$Y_n(y) = \sin(\beta_n y) + \frac{k\beta_n}{h} \cos(\beta_n y). \tag{7}$$

α_m and β_n are the solutions of equations

$$\frac{2h}{k\alpha - \frac{h^2}{k\alpha}} = \tan(\alpha L)$$

and

$$\frac{2h}{k\beta - \frac{h^2}{k\beta}} = \tan(\beta L).$$

$X_m(x)$ and $Y_n(y)$ are the eigenfunctions of Eq. (3) when $f(x, y) = 0$, and α_m and β_n are the corresponding eigenvalues of the eigenfunctions.

For convenient usage, the relevant physical properties of the lens in Eqs. (1)–(7) and the physical properties used in the flowing are shown in Table 1.

C. Balance Power Profile of Heating Devices

Before the realization of a specific aberration, it is necessary to find a set of power distributions to keep the lens at a uniform temperature higher than the working temperature of the optical system, such as 26°C. The balance power profile has two functions; on the one hand, it compensates for the heat dissipation from the lens edge to the lens frame and, on the other hand, it cancels out the heat dissipation from the lens surfaces to the cooling fluid.

For balancing heat dissipation from the lens edge to the lens frame, the most direct way is to use the electrical heating devices around the lens edge to heat the lens. Figure 5(a) shows the power distribution attributed to heat dissipation around the lens edge. Figure 5(b) shows the power profile of the heating devices for canceling out the heat flux from the lens surfaces to the cooling fluid. It can be easily obtained according to Fig. 3. By adding the power profiles mentioned above, Fig. 5(c) gives the total balance power profile on the lens surfaces.

It is worth noting that the source term $f(x, y)$ in Eq. (3) is not the heating flux of the heating devices; actually, it is the heat flux shown in Fig. 5(a). As depicted in previous sections, the heat flux of the heating devices in Fig. 5(b) is canceled out by the cooling fluid. Taking the heat flux shown in Fig. 5(a) as input, the temperature distribution of the lens can be easily calculated by Eqs. (4)–(7) provided in Section 3.B.

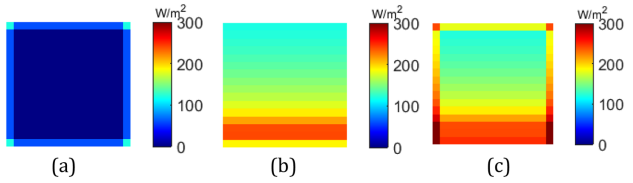

Fig. 5. Balance power distribution of the heating devices. (a) Power distribution for canceling heat dissipation from the lens edge. (b) Power distribution for canceling heat dissipation from the lens surface. (c) Total power distribution.

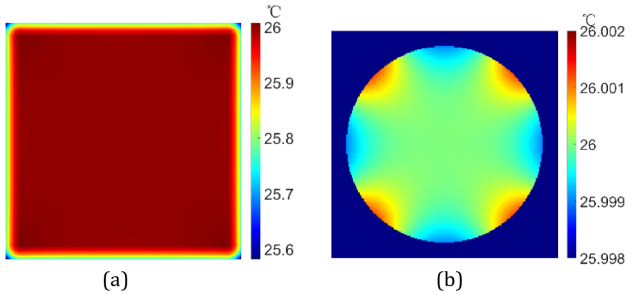

Fig. 6. Lens temperature due to the balance power. (a) Lens temperature of the whole lens and. (b) lens temperature inside the lens aperture.

Figure 6 shows the lens temperature. It can be seen that the temperature near the edge of the lens is lower than that in the center of the lens. However, inside the lens aperture, the lens temperature difference is no more than 2.2 mK. By adjusting the heating power around the balance power of each heating device, positive and negative power can be achieved on the lens surfaces. According to Fig. 3, the cooling heat flux on the lens surfaces is no more than 120 W/m^2, which would restrict the aberration modulation range of the apparatus.

D. Generation of Specific Aberrations

Since the apparatus is installed near the pupil of the optical system, it compensates for aberration offsets of the optical system. Thus, it is reasonable and convenient to approximate that the apparatus is illuminated by an ideal plane wave when we testify the modulation capability of the apparatus. The optical path difference (OPD) between the ideal plane wavefront and the modulated transmitted wavefront induced by the temperature profile can be calculated by

$$\mathrm{OPD}(x, y) = \frac{dn_{\mathrm{ref}}}{dT} \Delta T d, \tag{8}$$

where dn_{ref}/dT is the thermal coefficient of the lens material at 193.40 nm, ΔT is the lens temperature relative to 26°C. It can be easily inferred from Eq. (8) that the temperature profile and the modulated transmitted wavefront are the same except for a scale factor.

Specific aberrations can be achieved by adjusting the heating power of the heating devices individually. The implementation

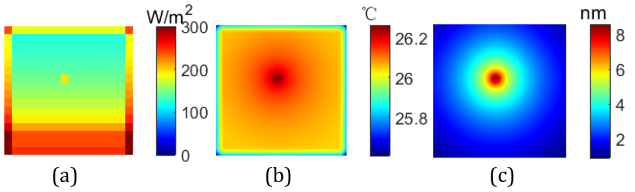

Fig. 7. Temperature response of a single heating device. (a) Heating power distribution when the adjusting heating device in the seventh row and eighth column. (b) Corresponding temperature response of the heating device. (c) Corresponding OPD caused by the temperature change.

can be roughly divided into two steps. The first step is to obtain the temperature response of each heating device under a certain power. According to Eqs. (3)–(7), the aberration profile z^{pq} induced by the pq^{th} heating device at $t=\infty$ can be expressed by

$$Z^{pq}=\frac{dn_{\mathrm{ref}}}{dT}d\sum_{m=1}^{M}\sum_{n=1}^{N}\frac{{\omega_{mn}}^{pq}}{a(\alpha_m+{\beta_n}^2)}X_m(x)Y_n(y), \tag{9}$$

where ${\omega_{mn}}^{pq}$ are the coefficients of eigenfunctions due to the heating power profile $f(x,y)$ induced by the pq^{th} heating device and calculated by Eq. (5c), and M and N are the maximum considered orders of eigenfunctions.

As an example, Fig. 7(a) shows the heating power profile by adjusting the heating device in the seventh row and eighth column to a power that is 50 $\mathrm{W/m^2}$ higher than the balance power depicted in Fig. 6. Figure 7(b) shows the corresponding temperature. Figure 7(c) gives the aberration profile Z^{pq} induced by the pq^{th} heating device. It should be noticed that the aberration profile Z^{pq} in Eq. (9) is not the aberration profile induced by the power distribution shown in Fig. 7(a). The aberration profile Z^{pq} represents the optical path change due to an increment of the heating power of the pq^{th} heating device relative to the balance power.

The second step is to calculate the heating power profile according to the specific aberrations. Suppose that the target aberration profile Z can be expanded into the superposition of eigenfunctions $X_m(x)Y_n(y)$, as shown in Eqs. (6) and (7):

$$Z=\frac{dn_{\mathrm{ref}}}{dT}d\sum_{m=1}^{M}\sum_{n=1}^{N}{\phi_{mn}}^{r}X_m(x)Y_n(y), \tag{10}$$

where ${\phi_{mn}}^{r}$ are the coefficients of eigenfunctions due to the temperature profile corresponding to the specific aberration profile Z and calculated by Eq. (5c). Now the problem becomes finding a set of coefficients v_{pq} to minimize the difference between $\sum_{pq} v_{pq}Z^{pq}$ and Z. The best way is to use the constrained linear least-squares, shown as follows:

$$\min_{x}\ \|C\cdot v-r\|_2^2 \ \text{such that}\ lb\le v\le ub. \tag{11}$$

In the above equation,

$$C=\left[r_{11}\ \cdots\ r_{pq}\ \cdots\ r_{PQ}\right] \tag{12a}$$

$$r_{pq}=\left[\frac{{\omega_{11}}^{pq}}{a({\alpha_1}^2+{\beta_1}^2)}\ \cdots\ \frac{{\omega_{mn}}^{pq}}{a({\alpha_m}^2+{\beta_n}^2)}\ \cdots\ \frac{{\omega_{MN}}^{pq}}{a({\alpha_M}^2+{\beta_N}^2)}\right]^{T_r}, \tag{12b}$$

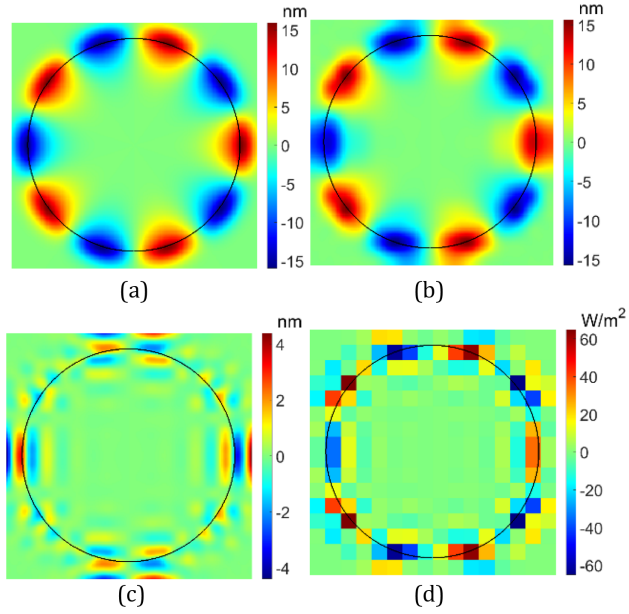

Fig. 8. Response of a specific aberration and corresponding power distribution. (a) Target aberration, (b) realized aberration, (c) difference between the target aberration and the realized aberration, and (d) corresponding power distribution.

$$r=\left[{\phi_{11}}^{r}\ \cdots\ {\phi_{mn}}^{r}\ \cdots\ {\phi_{MN}}^{r}\right]^{T_r}, \tag{13}$$

$$v=\left[v_{11}\ \cdots\ v_{pq}\ \cdots\ v_{PQ}\right]^{T_r}, \tag{14}$$

where T_r means the transpose of the matrix; v_{pq} is the heating power of the pq^{th} heating device relative to the balance power; lb and ub are the upper limit and lower limit of v, respectively; and P and Q are the maximum element number in the row and column, respectively.

As an example, Fig. 8 gives a specific aberration profile and corresponding power distribution calculated by Eqs. (9)–(14). The dark circle line in the figure represents the aperture of the lens. It can be seen from Fig. 8 that the error between the target aberration and the achieved aberration is mainly near the edge of the lens.

Figure 9 gives the apparatus response to the 16 Fringe Zernike settings. The Zernike coefficients are defined within the lens aperture, and only aberration profile data within the lens aperture are given. It can be seen from the figure that, as the aberration order increases, the difference between the ideal Zernike aberration and the achieved aberration becomes larger and larger. The main reason for this phenomenon is the limitation of the sizes and numbers of the heating devices.

E. Influences of the Heating Device Sizes and Numbers on the Generation of Specific Aberrations

In the previous section, we have discussed the method for a specific aberration generation using parameters discussed in Section 2. However, the influence of the heating device sizes and numbers on aberration accuracy have not been discussed yet. Thus, we carry out two cases of analysis as follows. One is

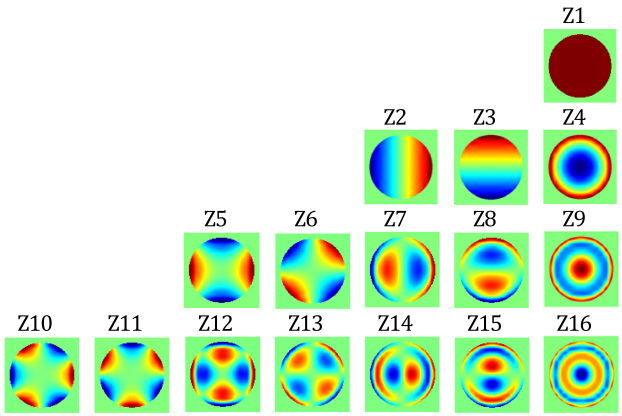

Fig. 9. Apparatus response to the 16 Fringe Zernike settings.

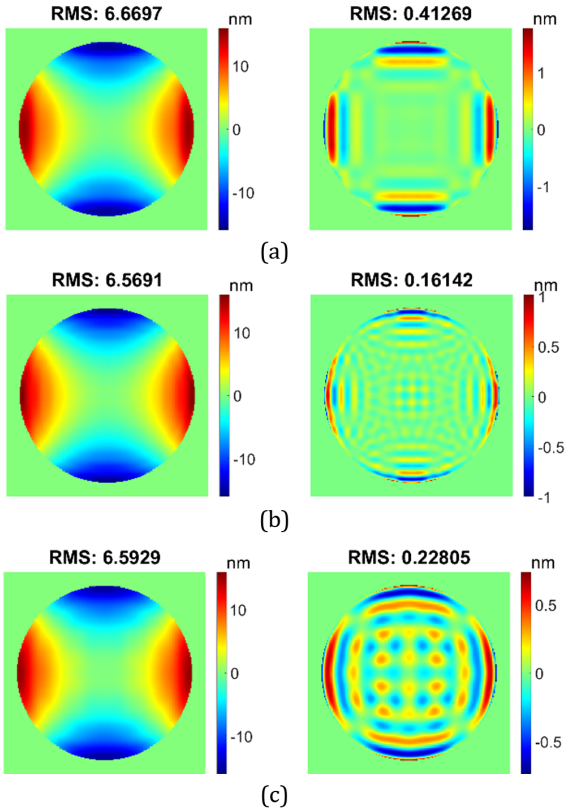

Fig. 10. Effects of the heating device sizes and numbers on aberration generation accuracy of Z5; the left columns are the obtained profiles, and the right columns are the deviation from the target profiles. (a) Size $6.5 \times 6.5\ \text{mm}^2$, number 16×16; (b) size $3.25 \times 3.25\ \text{mm}^2$, number 16×16; and (c) size $6.5 \times 6.5\ \text{mm}^2$, number 32×32.

that the size of the heating device remains the same, as shown in Fig. 1, while the number of heating devices is doubled, and the other is that the size of the heating device is reduced by two times, while the number is doubled. Z5 and Z16 are taken as examples to show the effects of heating device numbers and sizes on aberration generation accuracy, as shown in Figs. 10 and 11.

From Figs. 10 and 11, we see that the size reduction of the heating devices and the number increase of the heating devices will affect the magnitude and distribution of difference between

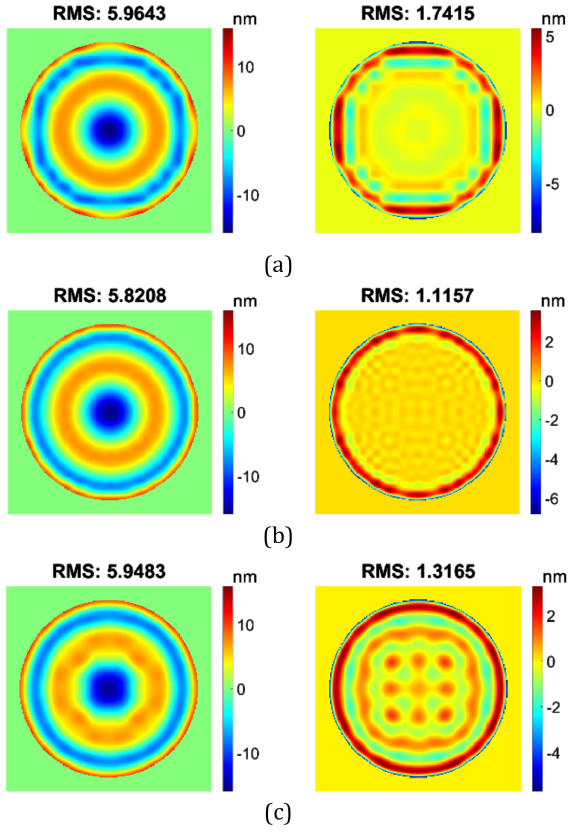

Fig. 11. Effects of the heating device sizes and numbers on aberration generation accuracy of Z16; the left columns are the obtained profiles and the right columns are the deviation from the target profiles. (a) Size $6.5 \times 6.5\ \text{mm}^2$, number 16×16; (b) size $3.25 \times 3.25\ \text{mm}^2$, number 16×16; (c) size $6.5 \times 6.5\ \text{mm}^2$, number 32×32.

target aberration and realized aberration. However, there is no significant reduction of error, especially for Z16. Considering the physical realization of the apparatus, the increment of the lens size and the number of heating devices will increase the difficulty of manufacturing. Thus, we still choose the number of heating devices provided in Ref. [21] to carry out the following analysis.

4. IMPLEMENTATION OF DYNAMIC THERMAL ABERRATION COMPENSATION

The essential principle of the compensator revealed in this paper is the cooling and heating of a plane plate lens in a desired way to generate specific aberrations. Different from the previous compensators, the aberration response to a specific power profile is not time-to-time due to the heat capacity of the lens. It takes several hours for the temperature of the lens to stabilize under a specific power distribution.

If the thermal aberration of the optical system is stabilized, we can set the heating power of each heating device as a fixed value to compensate for the stabilized aberrations. However, thermal aberrations of the optical system vary during the exposure process. Therefore, we should consider how to modulate power distribution to compensate for the dynamic thermal aberrations.

From Eq. (5a), we can see that the two terms on the right hand have clear physical meanings. The first term represents the effect

of the initial temperature on the temperature of the lens at t, and the second term represents the temperature distribution due to a specific heat load. If we discretize the actual transient aberration to N segments, we would find that the temperature distribution at time t_i and the temperature distribution at time t_{i+1} have the following relationship:

$$T_{mn}(t_{i+1}) = \phi_{mn}(t_i)e^{-a(\alpha_m{}^2+\beta_n{}^2)(t_{i+1}-t_i)} + \frac{\omega_{mn}(t_i)}{a(\alpha_m{}^2+\beta_n{}^2)}\left(1-e^{-a(\alpha_m{}^2+\beta_n{}^2)(t_{i+1}-t_i)}\right). \tag{15}$$

If we know the desired temperature profile $T_{mn}(t_{i+1})$ at time t_{i+1} and the realized temperature distribution $\phi_{mn}(t_i)$ at time t_i, we can calculate the power distribution we have to set at t_i as follows:

$$\omega_{mn}(t_i) = \frac{a(\alpha_m{}^2+\beta_n{}^2)}{\left(1-e^{-a(\alpha_m{}^2+\beta_n{}^2)(t_{i+1}-t_i)}\right)} \times \left(T_{mn}(t_{i+1}) - \phi_{mn}(t_i)e^{-a(\alpha_m{}^2+\beta_n{}^2)(t_{i+1}-t_i)}\right). \tag{16}$$

During the process of the dynamic thermal aberration compensation, we have to calculate the time-to-time temperature profile of the apparatus to compensate for the transient aberrations of the optical system. The process for the calculation of a desired temperature profile for transient aberration compensation is similar to the process of computer aided alignment (CAA) [22,23]. It is just that the compensators become the temperature profiles of heating devices and the compensation targets turn to be the thermal aberrations.

It is worth noting that the sensitivity of the temperature profile of each heating device should not be calculated by Eq. (8), since the apparatus is not exactly located in the pupil of the optical system and the laser beam is not collimated. The real ray trace method should be used to precisely calculate the aberration sensitivity of each heating device for every field point of the optical system.

If the specific temperature profile of the apparatus for each time has been obtained, then we can use Eqs. (15) and (16) to calculate the power distribution of the heating devices. As the number of heating devices and the size of the heating device are limited, the power profile represented in Eq. (16) might not be achievable. The least squares method should be used to fit the power profile to minimize the difference.

As an example, we implement the method provided above on the transient aberrations of a projection lens with NA of 1.35. The heating conditions of thermal aberrations are listed in Table 2, and both the heating and cooling times are 3 h. In our simulation, the time step $dt = t_{i+1} - t_i$ in Eq. (15) is 150 s.

Only transient aberrations at the central field of the projection lens are selected for illustration. The red line in Fig. 12 gives

Table 2. Heating Conditions of the Projection Lens

Mask	NA/sigma	Illumination Type	Wafer Power/W
Open frame	1.35/0.97/0.85	Dipole X 30°	0.16

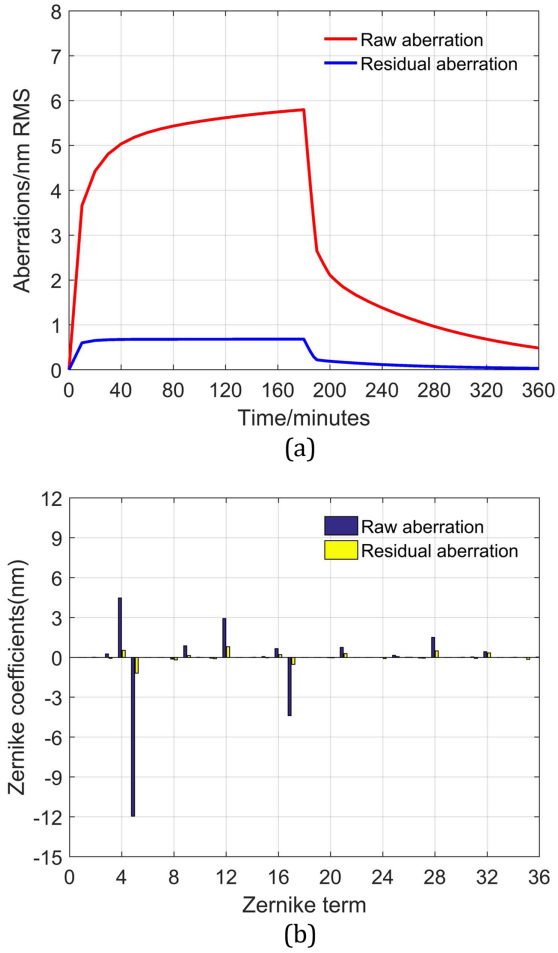

Fig. 12. Transient aberrations due to the heating and cooling of the projection lens and its residual aberrations after compensation by the apparatus provided in this paper. (a) Raw aberration and residual aberration curve. (b) Zernike coefficient distribution of raw and residual aberrations at $t = 3$ h.

the simulated raw transient aberrations of a heating and cooling process, while the blue line gives residual aberrations after compensation; similar results can be found in Refs. [1,3,4]. The maximum root mean square (RMS) value of the raw aberration is 5.80 nm and can be compensated to 0.68 nm RMS using the apparatus presented in this paper. The Zernike coefficient distributions of raw and residual aberrations at the time of 3 h are also provided in Fig. 12(b).

Figure 13 gives the temperature profiles and power profiles at different times. It can be seen from the figure that the temperature profiles at different times vary, and the corresponding power distributions are also different.

5. CONCLUSION

In this paper, we present an apparatus used for thermal aberration compensation in lithographic exposure tools. We first introduced the concept of the apparatus. The key point of the apparatus is that the cooling fluid at the operating temperature of the optical system is guided to cool an electrically heated lens. Therefore, by modulating the power of each individually addressable heating device, the temperature of the lens can be

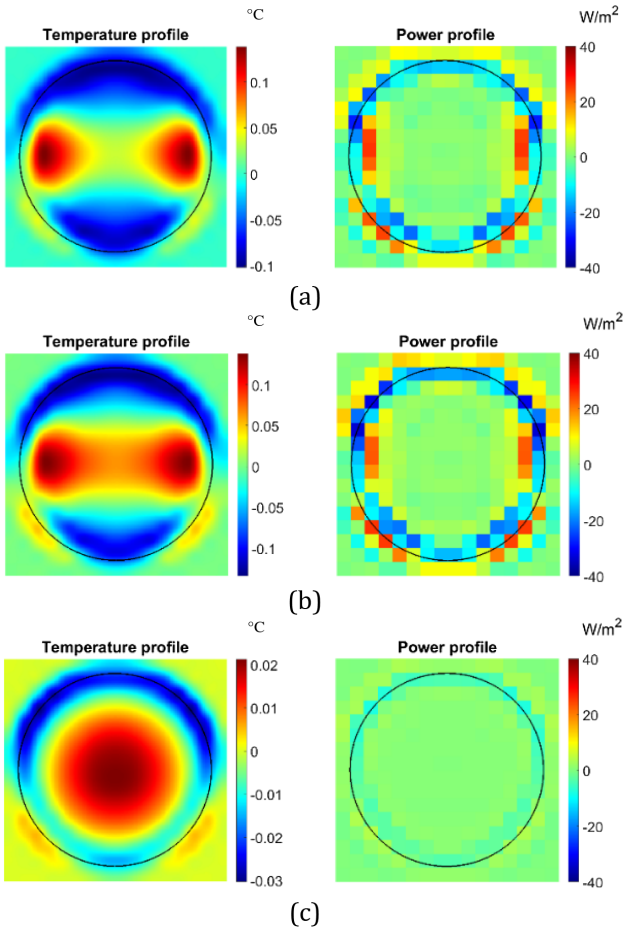

Fig. 13. Temperature profiles and corresponding power profiles: (a) $t = 1$ h, (b) $t = 2$ h, and (c) $t = 3$ h.

actively modulated in a desired way to compensate for thermal aberrations. The advantage of using cooling fluid at the operating temperature is that the thermal disturbance to the environment surrounding the apparatus can be minimized. However, the temperature of the lens must be heated to a higher level to maintain the cooling power of the lens. Then, based on the concept of the apparatus, we established an analytical model to describe the temperature of the lens and calculated the balance power profile to keep the lens at a temperature that is 4°C higher than the operating temperature. To prove the modulation ability of the apparatus, methods for a specific aberration generation and the apparatus response to the 16 Fringe Zernike settings were presented. At last, an algorithm to compensate for the dynamic thermal aberrations was established to overcome the time lag effects of the thermally controlled lens. Using the proposed algorithm, compensation simulations were performed on a transient aberration of an optical system. The results show that by dynamically adjusting the heating power of each heating device, the RMS wavefront error can be compensated from 5.8 nm to less than 0.68 nm across the entire transient process, which confirmed the effectiveness of the apparatus and our mathematical model.

Funding. Ministry of Science and Technology of the People's Republic of China (2009ZX02205); National Science and Technology Planning Project.

Disclosures. The authors declare no conflicts of interest.

Data availability. Data underlying the results presented in this paper are not publicly available at this time but may be obtained from the authors upon reasonable request.

REFERENCES

1. T. Nakashima, Y. Ohmura, T. Ogata, Y. Uehara, H. Nishinaga, and T. Matsuyama, "Thermal aberration control in projection lens," Proc. SPIE **6924**, 69241V (2008).
2. P. Liu, M. Snajdr, X. Zhang, Y. Cao, J. Ye, and Y. Zhang, "A computational method for optical application specific lens control in microlithography," Proc. SPIE **7640**, 76400M (2010).
3. T. Yoshihara, T. Sukegawa, N. Yabu, M. Kobayashi, T. Arai, T. Kitamura, A. Shigenobu, Y. Hasegawa, and K. Takahashi, "Advanced aberration control in projection optics for double pattering," Proc. SPIE **7274**, 72741L (2009).
4. T. Ohmura, T. Ogata, T. Hirayama, H. Nishinaga, T. Shiota, S. Ishiyama, S. Isago, H. Kawahara, and T. Matsuyama, "An aberration control of projection optics for multi-patterning lithography," Proc. SPIE **7973**, 79730W (2011).
5. Y. Fujishima, S. Ishiyama, S. Isago, A. Fukui, H. Yamamoto, T. Hirayama, T. Matsuyama, and Y. Ohmura, "Comprehensive thermal aberration & distortion control of lithographic lenses for accurate overlay," Proc. SPIE **8683**, 86831I (2013).
6. Y. Ohmura, Y. Tsuge, T. Hirayama, H. Ikezawa, and D. Inoue, "High-order aberration control during exposure for leading-edge lithography projection optics," Proc. SPIE **9780**, 97800Y (2016).
7. Y. Yoda, A. Hayakawa, S. Ishiyama, Y. Ohmura, I. Fujimoto, T. Hirayama, Y. Shiba, K. Masaki, and Y. Shibazaki, "Next-generation immersion scanner optimizing on-product performance for 7nm node," Proc. SPIE **9780**, 978012 (2016).
8. J. Mulkens, J. Klerk, M. Leenders, F. Jong, and J. W. Cromwijk, "Latest developments on immersion exposure systems," Proc. SPIE **6924**, 69241P (2008).
9. I. Bouchoms, A. Engelen, J. Mulkens, H. Boom, R. Moerman, P. Liebregts, R. Graaf, M. Veen, P. Thomassen, W. Emera, and F. Sperling, "Extending single-exposure patterning towards 38-nm half-pitch using 1.35 NA immersion," Proc. SPIE **7274**, 72741K (2010).
10. F. Staals, A. Andryzhyieuskaya, H. Bakker, M. Beems, J. Finders, T. Hollink, J. Mulkens, A. Nachtwein, R. Willekers, P. Engblom, T. Gruner, and Y. Zhang, "Advanced wavefront engineering for improved imaging and overlay applications on a 1.35 NA immersion scanner," Proc. SPIE **7973**, 79731G (2011).
11. M. A. Arain, W. Z. Korth, L. F. Williams, R. M. Martin, G. Mueller, D. B. Tanner, and D. H. Reitze, "Adaptive control of modal properties of optical beams using photothermal effects," Opt. Express **18**, 2767–2781 (2009).
12. Z. Liu, P. Fulda, M. A. Arain, L. Williams, G. Mueller, D. B. Tanner, and D. H. Reitze, "Feedback control of optical beam spatial profiles using thermal lensing," Appl. Opt. **52**, 6452–6457 (2013).
13. P. Berto, L. Philippet, J. Osmond, C. F. Liu, A. Afridi, M. M. Marques, B. M. Agudo, G. Tessier, and R. Quidant, "Tunable and free-form planar optics," Nat. Photonics **13**, 649–656 (2019).
14. M. A. Arain, V. Quetschke, J. Gleason, L. F. Williams, M. Rakhmanov, J. Lee, R. J. Cruz, G. Mueller, D. B. Tanner, and D. H. Reitze, "Adaptive beam shaping by controlled thermal lensing in optical elements," Appl. Opt. **46**, 2153–2165 (2007).
15. R. Lawrence, D. Ottaway, M. Zucker, and P. Fritschel, "Active correction of thermal lensing through external radiative thermal actuation," Opt. Lett. **29**, 2635–2637 (2004).
16. A. Haber, J. E. Draganov, K. Heesh, J. Tesch, and M. Krainak, "Modeling and system identification of transient STOP models of optical systems," Opt. Express **28**, 39250–39265 (2020).
17. A. Haber, J. E. Draganov, K. Heesh, J. Cadena, and M. Krainak, "Modeling, experimental validation, and model order reduction of mirror thermal dynamics," Opt. Express **29**, 24508–24524 (2021).
18. A. Haber, A. Polo, S. Ravensbergen, H. P. Urbach, and M. Verhaegen, "Identification of a dynamical model of a hermally actuated deformable mirror," Opt. Lett. **38**, 3061–3064 (2013).

19. A. Haber, A. Polo, I. Maj, S. F. Pereira, H. P. Urbach, and M. Verhaegen, "Predictive control of thermally induced wavefront aberrations," Opt. Express **21**, 21530–21541 (2013).
20. L. Hahn and P. Eberhard, "Transient dynamical-thermal-optical system modeling and simulation," J. Eur. Opt. Soc. **17**, 5–9 (2021).
21. B. S. H. Jansen, E. R. Loopstra, M. Ravensbergen, and M. J. Hauf, "Lithography apparatus and device manufacturing method," EP patent 1 921 505 B1 (February 23, 2011).
22. K. Liu, Y. Li, J. Liu, and C. Kuang, "Computer aided alignment of a 20X Schwarzschild projection optics," Proc. SPIE **7130**, 713042 (2008).
23. L. Li, X. Fu, T. Ma, and B. Wang, "Computer-aided alignment for high precision lens," Proc. SPIE **9282**, 92820Y (2014).